ORIGINAL PAPER

Activation of PET Using an RF Atmospheric Plasma System

Mick Donegan · Vladimir Milosavljević · Denis P. Dowling

Abstract The plasma treatment of polymer surfaces is routinely used to enhance surface properties prior to adhesive bonding or biomolecule interaction. This study investigates the influence of plasma treatment conditions on the surface activation of polyethylene terephthalate (PET) using the SurFx Atomflo™ 400L plasma source. In this study the effect of applied plasma power, processing speed, gas composition and plasma applicator nozzle to substrate distance were examined. The level of polymer surface activation was evaluated based on changes to the water contact angle (WCA) of PET samples after plasma treatment. PET surface properties were also monitored using surface energy and X-ray photoelectron spectroscopy (XPS) analysis. The heating effect of the plasma was monitored using thermal imaging and optical emission spectroscopy (OES) techniques. OES was also used as a diagnostic tool to monitor the change in atomic and molecular species intensity with changes in experimental conditions in both time and space. XPS analysis of the PET samples treated at different plasma powers indicated that increased oxygen content on samples surfaces accounted for the decreases observed in WCAs. For the first time a direct correlation was obtained between polymer WCA changes and the OES measurement of the atomic hydrogen Balmer H_α and molecular OH line emission intensities.

Keywords Atmospheric plasma jet · Surface activation · Polyethylene-terephthalate · XPS · Optical emission spectroscopy

M. Donegan · D. P. Dowling
School of Mechanical and Materials Engineering, University College Dublin, Belfield, Dublin 4, Ireland

V. Milosavljević (✉)
NCPST and School of Physics, Dublin City University, Dublin 9, Ireland
e-mail: vm@dit.ie; vladimir@ff.bg.ac.rs

V. Milosavljević
Faculty of Physics, University of Belgrade, Belgrade, Serbia

Introduction

Polyethylene terephthalate (PET) is widely used in a variety of industries from food packaging to the electrical, electronics, and biomedical industries [1–5]. The chemical inertness and low surface energy of polymers [6] in general can lead to difficulties in laminating, coating, packaging, dyeability and cell attachment. To address this issue, a large range of techniques has been used to modify the surfaces of polymeric materials: chemical treatments [7, 8], corona [9], glow discharge [10], dielectric barrier discharge [2, 11, 12], blown arc [13] and rf plasma treatments [14–17]. The surface properties of PET are known to respond well to non-thermal plasma treatments in particular [3]. There are many advantages to the use of atmospheric plasma treatment for the activation of polymers including the uniformity of the treatment [18], the ease in which they can be easily integrated into existing production lines and that they can treat specific parts of selected substrates [19]. Atmospheric plasma treatment of surfaces is a dry, environmentally clean process, where the depth of polymer modification is generally below 10 nm [20]. Plasma treatment has the effect of surface oxidation by introducing functional groups containing oxygen into the molecular chains of PET [3]. This occurs due to the chain scissoring of the long polymer molecules, generating potential bond sites for the oxygenated functional groups [21, 22].

The level of polymer activation generally increases with the applied power to the plasma, however this increase in power is also associated with and increase in plasma temperature [23]. Polymers, such as PET, are thermally damaged at relatively low temperatures and so a delicate balance must be reached where surface activation of the polymer is maximised, while thermal damage is prevented. This paper has a particular focus on the use of plasma diagnostic techniques (optical emission spectroscopy and thermal imaging) and to correlate these to the changes in PET properties as a result of plasma surface treatments. Sources operating at 27.12 MHz at low-pressure have also previously been used to activate PET surfaces [24–26]. These papers report a large decrease in the water contact angle (WCA) of PET samples when treated with oxygen plasma, while XPS analysis of their samples indicated increased oxygen content on the surfaces of the PET after the plasma treatment. Other plasma treatment studies of PET report increased nano-particle adsorption on activated surfaces [27], bio-deactivation of bacteria [28], suppressed blood platelet adhesion [29], increased adhesion of antibacterial coatings [30], increased surface wettability [31], deposition of films that tailor the water permeability of PET membranes [32] and increased heat-sealing bond strengths [33].

This paper examines the influence of plasma processing conditions on the performance of the SurFx source. The treatment studies were carried out using the SurFx Atomflo^{TM} 400L plasma source, which operates at 27.12 MHz, with a 5 cm linear beam applicator (AH-500L) (Fig. 1). Only one study has been published to date on this model of the SurFX source. It involved the pre-treatment of cotton to enhance the bonding of a flame retardant coating [34]. The performance of older SurFx system designs have however been reported for example to evaluate the effect of He–O$_2$ plasma on the activation of polymers [35, 36]. In this paper a more in-depth study is reported on the fundamental mechanisms of plasma-surface activation, by correlating plasma species intensities with changes in polymer surface properties. In particular this work investigates the effect on the WCA of PET with changes in system input power/gas flow rate. This information is in-turn correlated with changes in peak intensity observed by optical emission spectroscopy.

Fig. 1 Photograph of SurFx Atomflo^{TM} plasma applicator head. Operating conditions: Power 180 W, Helium = 30 l min⁻¹, O₂ = 0.8 l min⁻¹

Equipment and Procedures

SurFx Atomflo^{TM} 400L Atmospheric Plasma System

The SurFx Atomflo^{TM} 400L atmospheric plasma system operates at a frequency of 27.12 MHz a plasma is applied through the 5 cm wide AH-500L beam applicator. The unit can generate plasma using both He–O$_2$ and He–N$_2$ gas mixtures (in the range of 100–200 and 100–150 W respectively, which are the operational limits of this plasma source). The plasma applicator is mounted on a computer numeric control (CNC), the speed of which was set to either 250 or 30 mm s^{-1}. For a 1×1 cm sample, these CNC speeds are equivalent to treatment times of 0.08 and 0.70 s respectively, per pass of the plasma jet. In the course of this study a He–O$_2$ plasma was employed due to the requirement to oxidise polymer surfaces. The input variables on this system were limited by SurFx, otherwise system warranty was voided; helium gas needs to flow at a constant flow rate of 30 l min^{-1}, while secondary gas input with plasma power is set by the manufacturer (Table 1). The benefit of such a system is that, due to the high gas flow rate, the plasma discharge is very stable (no arcing), while plasma chemistry is dominated by the input gas mixture (He–O$_2$) with minimal contamination from ambient air (which is very difficult to achieve in a typical open air plasma discharges). Small differences in the oxygen flow rate result in a significant change in polymer surface properties [16]. Oxygen, in the majority of open-air discharges, is responsible for arcing and plasma instability, changing the RF power with oxygen gas flow rates prevented this from occurring. In general, commercial plasma tools give high reproducibility over the long period of an experimental run. The system is designed for surface treatments at plasma source-substrate distances of 3–15 mm.

Polymer Samples

Polyethylene terephthalate (PET) samples (dimensions 10×10 mm and 60×90 mm, 250 μm thick, molecular weight 192.2 g mol^{-1}) were used for surface activation trails. This polymer was selected as a suitable candidate for activation trials as it is widely used in the food packaging industry and has been investigated by other atmospheric plasma treatment systems [16, 37, 38]. After plasma treatment the polymer samples were stored in ambient air inside sealed petri dishes.

Table 1 Gas flow rates specified for the operating powers shown

Power (W)	He flow ($1 \ min^{-1}$)	O_2 striking flow ($1 \ min^{-1}$)
100	30	0.15
110	30	0.25
120	30	0.30
130	30	0.40
140	30	0.50
150	30	0.55
160	30	0.65
170	30	0.75
180	30	0.80
190	30	0.90
200	30	0.95

Thermal Analysis

Infrared thermal imaging of both the plasma applicator nozzle and the treated surface were obtained using an InfraTec Vari CAM high resolution infrared thermographic camera. The measurement procedure is similar to that reported previously [23]. Tests were carried out using both a thermal camera and a K-type thermocouple [13]. Thermal data was obtained while the plasma applicator head was mounted 16 mm above an alumina ceramic surface. After ignition of the plasma the change in ceramic and plasma applicator surfaces were recorded until a steady state maximum temperature was reached. This was repeated for all process powers described in Table 1 for the He–O_2 plasma. An alumina ceramic (W) 21 cm, (L) 27 cm and (H) 0.4 cm was chosen as the comparative substrate as it has a high specific heat capacity ($850 \ J \ g^{-1} \ K^{-1}$) [13] and thus avoids any thermal degradation issues that can occur for polymer surfaces after extended exposure to the discharge.

Optical Emission Spectroscopy (OES)

The optical emission from the plasma discharge was recorded using an Ocean Optics USB4000 UV/VIS spectrometer. The USB4000 obtains measurements in the 200–850 nm region of emissions, with a resolution of about 1.2 nm full width at half maximum (FWHM). A qualitative overview of the plasma chemistry is obtained by analysing the observed atomic spectral lines and molecular band emission intensities. Due to the relatively low intensity of the plasma emitted by the SurFx applicator, an optical lens was mounted on a specially constructed bracket directly under this plasma applicator head.

Using OES, the rotational temperature was measured from intensities of components of the R_2 branch of the (0,0) band for the electronic transition OH radical, i.e. $OH(A^2\Sigma^+) \rightarrow OH(X^2\Pi)$ band head at 306.357 nm, and it is close to the gas temperature [39]. OES data obtained under specific processing conditions were compared with thermal imaging data collected under similar experimental conditions. These spectra show a red degradation with four main band heads at 306.357 (R1), 306.766 (R2), 307.844 (Q1) and 308.986 (Q2) nm [39].

Water Contact Angle and Surface Energy Measurements

A Dataphysics Instruments OCA 20 Video Based Contact Angle Device, which utilises the sessile drop technique, was used to obtain WCAs, at room temperature. 1 µl drops were allowed to sit on the surface for 5 s (approx.) before WCAs were measured. This was carried out both immediately after plasma treatment and at varying times after treatment, in order to determine the rate of hydrophobic recovery [40]. Measurements were taken from three points on each of the samples. This was repeated for all of the polymers processed. Surface energies (SE) were determined using deionised water, diodomethane and ethylene glycol. Their contact angles were also taken at three different locations for each of the polymers tested. The OWRK method was then employed to calculate the surface energy of the polymers [41, 42].

X-ray photoelectron spectroscopy

X-ray photoelectron spectroscopy (XPS) analysis of the samples was carried out using a VG Microlab 310-F electron spectrometer. The photoelectrons were exited with an x-ray source using MgKα (hν = 1,253.6 eV) and the pass energy of the analyser was 20 eV yielding a resolution of 1.1 eV. The C1s and O1s peaks were recorded along with 50–1,000 eV survey scans. The intensities of the peaks were determined as the integrated peak areas assuming the background to be linear. XPS analysis was carried out on both the untreated and plasma treated samples of the PET polymer. Analyses were carried out 24 h after plasma activation of the polymer samples to allow the evacuation of the XPS analysis chamber.

Results and Discussion

Optical Emission Spectroscopy

Optical emission spectroscopy was used to investigate species intensity with varying power, time and axial location. This resulted in a matrix of 64 experiments. OES data was recorded at $x_1 = 1.25$, $x_2 = 2.5$ and $x_3 = 3.75$ cm along the 5 cm long plasma discharge opening for all the allowable system powers (Fig. 2). This allowed the spatial homogeneity of the plasma to be evaluated. OES data was also recorded, at the central (x_2) point along the axis, at 0, 15, 30, 45, 60 and 75 s after the plasma was struck, for all plasma powers.

Fig. 2 Schematic of SurFx Plasma System $X_1 = 1.25$ cm, $X_2 = 2.5$ cm, $X_3 = 3.75$ cm
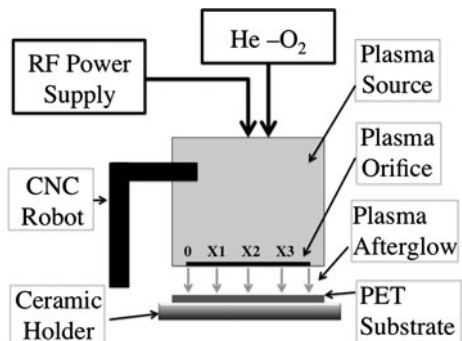
A typical He–O$_2$ OES spectrum, recorded at 180 W after 15 s at the centre of the SurFx applicator orifice (x$_2$) is given in Fig. 3. Using the Ocean Optics system, 13 different atomic and molecular species were observed in the obtained spectral emission from the He–O$_2$ plasma. In order provide an indication of the relative sensitivity of specific species to plasma processing conditions, the area under each OES peak was integrated [43]. The OES spectra recorded for seven individual plasmas which were repeatedly formed at 180 W, indicated good reproducibility of the OES measurements. The relative intensities were calculated to fall within a rage of 2.9 %, with a standard deviation of less than 1 %.

The integrated values (area) could then be compared to each other, thus allowing the species intensities (and change of these intensities) to be compared [43]. All species intensities were observed to change with increasing power. It appeared that the atomic helium triplet spectral lines HeI 587.56 nm (transition 2p-3d and multiplet $^3P°_{1,2}$–$^3D_{1,2,3}$), HeI 706.52 nm (transition 2p-1s and multiplet $^3P°_{0,1,2}$–$^3S_1$), as well as a helium singlet spectral line HeI 667.82 nm (transition 2p-1s and multiplet $^1P°_1$–$^1D_2$), and oxygen triplet OI at 777 nm (transition 3s-3p, and multiplet $^5S°_2$–$^5P_{3,2,1}$) species are most affected by the change of power applied to the plasma. Normalising this data however reveals more clearly the effect of increasing power on species intensities (Fig. 4). Normalisation was carried out by dividing the recorded intensities for each of the species by the maximum value observed for each species. The normalised data indicates that the atomic helium triplet (388.86, 587.56, 706.52 nm), and singlet (501.57, 667.81, 728.14 nm) spectral lines experience the largest increase in intensities with increasing power. HeI 667 in particular sees an 80 % increase in intensity from 100 to 200 W while OI 777 (the largest peak in Fig. 3) sees approximately half of that increase. Species intensity generally increased with applied power however, this trend was not always observed. In the case of the OH molecule emission, Balmer H$_α$ spectral line emission (λ = 656.28 nm, transition 2–3) and N$_2$-II+ i.e. molecular nitrogen second positive system (λ = 337.71 nm, transition $C^3\Pi_u^+$-$B3\Pi_g^+$, vibration band 0–0), intensities were much higher at 120 and 180 W plasma powers than adjacent powers. This may be due to system resonance and is an important factor in the treatment of surfaces with the plasma.
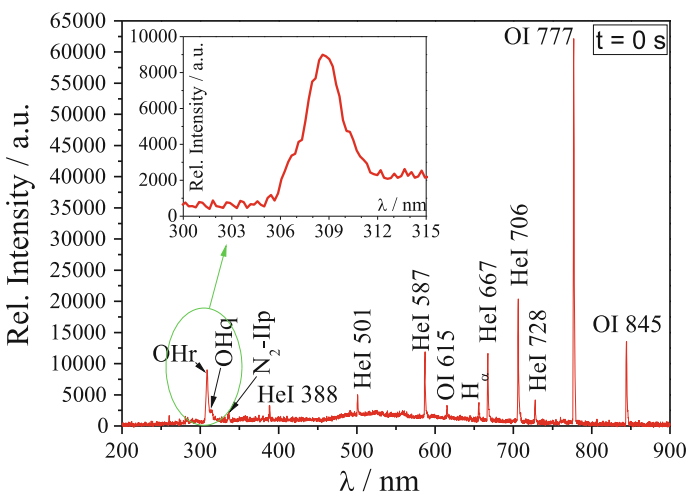

Fig. 3 Atomic and molecular species in He–O2 plasma at 180 W. The enlarged ranged spectra *inset* image shows the OH branches in the spectral range of 300–315 nm
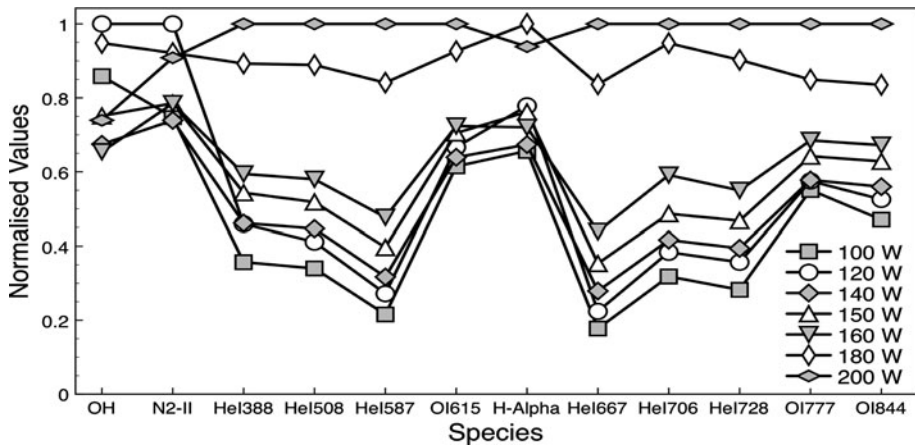
Fig. 4 Atomic and molecular species intensities at different powers shown. The intensities are obtained for the lines shown except in the case of OH where the peaks at 306 and 309 nm are detailed. In the case of N2-II and the H-Alpha lines the intensity is obtained from the peak at 337 and 656 nm respectively

In order to gain an insight into plasma homogeneity across the discharge, species intensity values were plotted against power and axial location in contour plots. Some general trends were observed; the species intensities were highest at the 2.5 cm (centre of plasma generation orifice) location. Either side of this (at 1.25 and 3.75 cm) the intensities decreased (by over to 50 % for OH species at 120 W) at like-for-like powers. Interestingly the 1.25 cm location generally recorded lower species intensities than the 3.75 cm location, especially at powers below 150 W. These observations would indicate that some non-uniformity in the level of plasma activation across the polymer surface may occur across the 5 cm polymer surface. In order to investigate this, further thermal imaging studies were carried out.

Thermal Analysis

Thermal imaging analysis, in the infrared spectra, was carried out using an InfraTec Vari CAM high-resolution infrared thermographic camera. The plasma applicator head was moved into position, 16 mm above an alumina ceramic surface, for this series of experiments.

The plasma was ignited and the change in temperature of the alumina ceramic surface and plasma applicator surface was recorded until a steady state maximum temperature was reached. An InfraTec IRBIS3 plus software package was used to generate plots of the maximum steady state temperatures for $He–O_2$ plasmas from 100 to 200 W (in 10 W increments). Figure 5 shows the two lines along which the data was examined for the temperatures of both the SurFx applicator's surface (L1) and ceramic test surface (L2). Table 2 shows the maximum steady state temperature reached (after a treatment time of 2 min) along the nozzle and the ceramic. These processing temperatures are an important consideration when treating thermally sensitive materials, such as PET.

The 55 °C maximum steady state temperature observed on the substrate, for this $He–O_2$ plasma, compares favourably with the 85 °C observed using the PlasmaTreat[TM] air plasma system for the same treatment time and gap height over the same ceramic plate [13].

Fig. 5 *Black lines* showing the positions at which thermal data was obtained: Plasma Nozzle (*L1*) and ceramic substrate (*L2*) (viewed from above). The distance between L1 and L2 is 16 mm
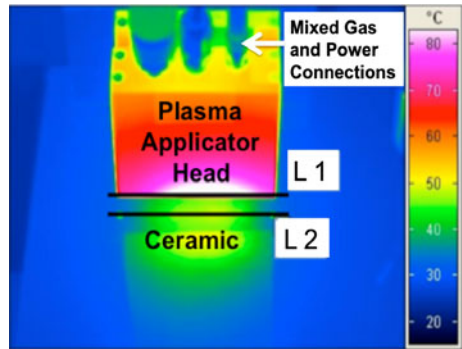

Table 2 Maximum temperatures reached after 2 min of processing

Power (W)	Max Temp. nozzle (°C)	Max Temp. ceramic (°C)
100	56	36
120	65	40
140	80	42
160	91	49
180	103	54
200	113	56

Generally He based plasmas yield lower temperature plasmas compared with those formed in air due to the relatively low input power requirement of He plasmas. The OES technique was used to measure the rotational temperature of the OH molecules. This allowed a comparison of thermal imaging of the applicator head and OES analysis of the plasma for the purpose of estimating plasma gas temperatures [39].

The intensity of an individual spectral line, where the rotational structure of a band depends on the line intensity for that particular line, depends on the population of molecules in the initial state and another factor, which is common to all lines in the same band [39]. One may assume that, in rotational relaxation, collisions between molecules are dominant. If no self-absorption or superposition of lines occur, then the temperature of the plasma can be determined from line intensities using a Boltzmann plot, or the intensity ratio of two lines, which originate from the same transition. In order to decrease the uncertainty in the calculated temperature, transitions with large energy differences should be used. This method is of great interest as the uncertainty in the measured continuous background is small and so no spectral sensitivity calibration of the optical system is needed if emission lines are similar in wavelength. The following four main OH band heads at 306.357 (R1), 306.766 (R2), 307.844 (Q1) and 308.986 (Q2) nm, are used for this purpose throughout this work. A typical emission spectrum at 300–315 nm is shown in Fig. 3 (insert).

The OES spectra used for analyses (shown earlier in Fig. 3) were taken 15 s after the plasma was ignited. These temperatures are compared with the spectroscopic thermal data of the plasma applicator nozzle recorded for the same time period. Figures 6, 7 and Table 3 show that there is good agreement between the temperature recorded by the thermal imaging and OES techniques. There is an offset in the temperatures recorded by the different techniques, which, may have been due to heat conduction from the plasma

through the metal plasma applicator. Temperatures were observed to increase with applied system power (Fig. 6) while Fig. 7 demonstrates how temperature increases with time at a specific power, in this case 180 W.

Further investigation was also carried out into the homogeneity of the plasma across the applicator's orifice. Table 3 shows good agreement between the OES and thermal analysis data demonstrating that the area on the left hand side of the applicator was approximately 11 °C cooler than the centre of the applicator nozzle 15 s after igniting the plasma. Here again the offset between the thermal imaging and OES data is in the range of 3–5 °C.

Effects of Plasma Treatment on PET Water Contact Angle

PET samples were activated using a helium–oxygen plasma. Before surface treatment the PET samples were cleaned ultrasonically using methanol and then allowed to air dry. Three different treatment parameters were initially investigated: plasma power (120 and 180 W gas flow rates set out in Table 1), source to substrate distance (5, 10, 15 and 20 mm) and a single pass of the jet at a CNC speed of 250 and 30 mm s^{-1}. In total 14 differently activated surfaces were obtained using these parameters. WCA testing was carried out on these samples at 1, 24 h and 5 days after surface activation, to determine initial changes in WCA and subsequent hydrophobic recovery [40]. The general trends resulting from this investigation are as follows: a large spread in WCA was obtained for the activated polymers. Low plasma power, high gap height and a rapid CNC speed produced

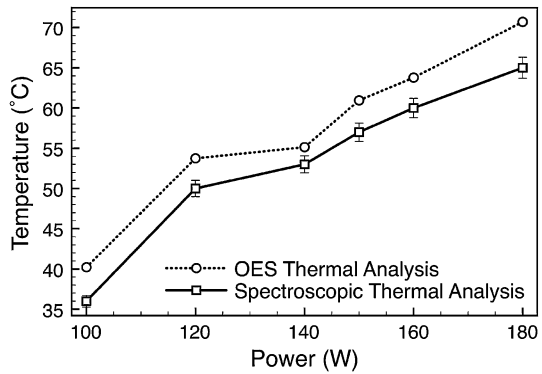**Fig. 6** Temperature of plasma and plasma applicator nozzle, after 15 s, at the input powers shown

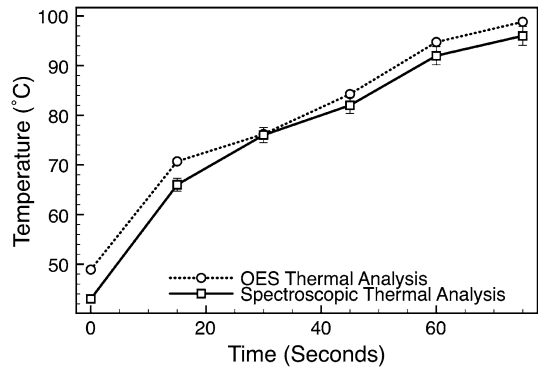**Fig. 7** Infrared and OES thermal analysis of He–O$_2$ plasma at 180 W as a function of time

Table 3 Infrared and OES thermal analysis based on axial position 15 s after plasma ignition

| Position reading (mm)	12.5	25	37.5
Thermal imaging (°C)	59	71	69
OES thermal analysis (°C)	56	66	65

no significant change in WCA compared with that of the untreated polymer (93°). As plasma power increased, gap height decreased and CNC speed was reduced, a marked difference with WCA was observed. The lowest WCA obtained, of 34°, is similar to the level reported after the plasma activation of PET by other authors [35, 37].

From this investigation it is concluded that high plasma powers, low gap heights and slower CNC speeds were required in order to sufficiently activate the surface of PET samples. The optimised conditions were:

$$\text{Power}: 180 \text{ W} \quad \text{CNC Speed}: 30 \text{ mm sec}^{-1} \quad \text{Gap Height}: 5 \text{ mm}$$

Following the OES and thermal analysis of the SurFx system, it was decided to investigate how the non-uniformity in the thermal and atomic/molecular species homogeneity across the plasma discharge affected WCA. PET samples with dimensions 90×60 mm, were treated using the optimised conditions. WCAs were measured at 5 mm intervals; perpendicular to the direction that the CNC traversed over the polymers surface after this treatment. Figure 8 (top) shows the average WCAs obtained for three PET samples, which were treated using the plasma plume. Relatively uniform plasma activation of the PET surface is evident for a width of approximately 60 mm and begins approximately 5 mm either side of the where the plasma orifice passed over the polymer. A sharp decrease in WCA is observed in comparison to the untreated PET, with WCAs dropping from 93° (untreated PET) to 49° and 45°, 5 mm from the left and right edges respectively. This difference in WCA, equidistant from the edges of the plasma plume, concurs with the thermal and OES observations that the plasma is not fully uniform across the discharge. WCAs continued to decrease as the measurements approached the centre where the WCA averaged 34° (stdev. 1.2). Figure 8 (bottom) shows a photograph of 5 μl water drops dispensed across the polymer surface 1 day after it was plasma activated. Note how the two droplets at either untreated edge are hemispherical while the droplets on the plasma

Fig. 8 WCA measurements across PET polymer obtained after a single pass of the SurFx source. Values ranged from 34° to 47° after treatment under the 5 cm jet orifice (*top*). Photograph of water droplets placed on the treated and untreated polymer, demonstrating their hydrophilic and hydrophobic (beaded droplet) respectively (*bottom*)
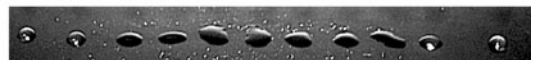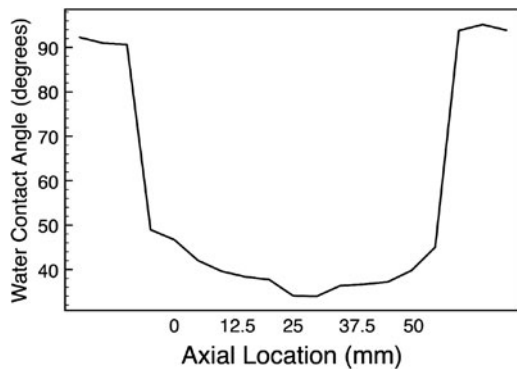
activated section spread out across the surface of the polymer due to the increase in surface energy.

The hydrophobic recovery of the treated PET polymers was investigated up to a 15-day period. This time line was chosen as it has previously been used in other plasma activation studies [13]. Figure 9 shows the WCA of polymer samples activated at the different plasma powers shown. A general trend is seen where an increase in power results in a decrease in WCA. The rate of hydrophobic recovery is similar to that reported previously for PET treated with He–O_2 plasmas [16].

Samples that were treated at 120 and 180 W were notable in that they displayed WCA that were lower than those at the powers adjacent to them. The rate of hydrophobic recovery for the PET treated at an input power of 120 W is also more rapid for the first 24 h post treatment than for any other process treatment power. In order to investigate why this may be the case further analysis of OES data of the plasma was conducted. Based on an analysis of the resulting spectra it was noted that the molecular and atomic species generally increased in intensity with applied power. This trend was not observed however, for the spectra recorded at 120 and 180 W where OHr and OHq branches of the OH molecule, H_α and molecular nitrogen N_2-II+ emissions were higher than for other adjacent powers. It is possible that these species, or a combination of said, played a major role in the modification of the polymer surfaces and so the increase of these species at 120 and 180 W resulted in the relatively low WCA observed for PET processed at these powers. It is known that ambient moisture levels effect the level of activation of hygroscopic polymers [36]. The increase of observed species intensities at 120 and 180 W, particularly OH and H_α, may indicate that atmospheric water vapour experiences more dissociation at these powers than at adjacent powers, resulting in increased levels of activation. By normalising the change in polymer WCA (normalised by observed change in WCA), OH and H_α (normalised by maximum intensity) and plotting these against power it can be observed that there is good correlation between the normalised WCA and H_α values (Fig. 10), while the normalised OH intensities follow a similar trend. Statistical analysis indicates a 96 % correlation between the normalised change in polymer WCA and H_α intensity values. This correlation may indicate that OES peak intensities can be used as an indicator of treated polymer WCA, without the need for conventional off-metrology.

The surface energy of PET polymer samples was correlated with the WCA measurements (Fig. 11), in which surface energy is shown by dashed lines and WCA by solid lines. As expected for the treatments shown at 120 and 180 W, there is a direct correlation between the WCA increase and the SE decrease. The relationship between surface energy and WCA has also been reported previously for plasma deposited coatings [44].

Fig. 9 Hydrophobic recovery observed up to a 15 day period for PET treated using the SurFx system operated at the different processing powers shown
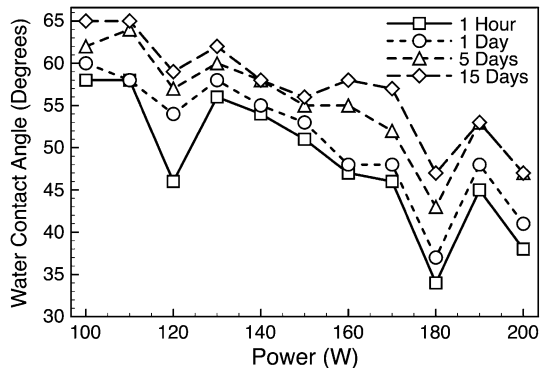
Fig. 10 Normalised change in WCA 1 h and 1 day post activation and H_α intensity versus system power
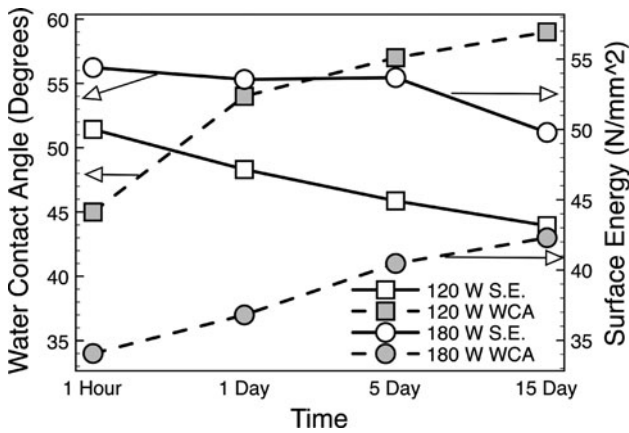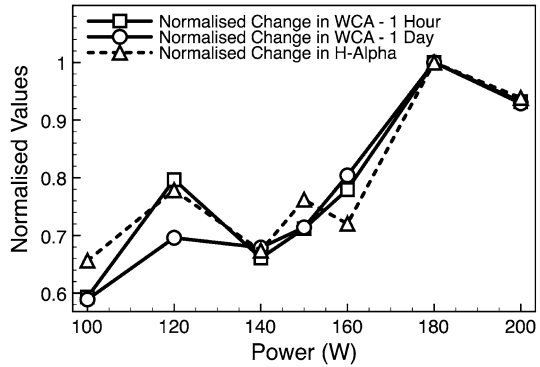

Fig. 11 Correlation between surface energy and WCA measurements for PET polymers plasma treated at 120 and 180 W

Table 4 PET substrate XPS results obtained both prior to and also post treatment for three different plasma power settings (120, 150 and 180 W)

Power	% C	% O
Untreated	80.3	19.7
120 W	70.6	29.4
150 W	68.9	31.1
180 W	65.9	34.1

XPS Analysis

X-ray photoelectron spectroscopy (XPS) analysis was carried out on untreated and plasma treated samples using the plasma processing powers outlined in Table 4. The C1s and O1s peaks were recorded along with 50–1,000 eV survey scans, 24 h after plasma activation. The intensities of the peaks were determined as the integrated peak areas assuming the background to be linear. The theoretical atomic percentages of carbon to oxygen atoms on untreated PET should be 71.4 and 28.6 % respectively. XPS reveals the values of carbon and oxygen on the untreated PET samples to be 80.3 and 19.7 % indicating a slight

Fig. 12 High resolution C1s XPS analysis of PET surface pre and post surface activation at 120, 150 and 180 W
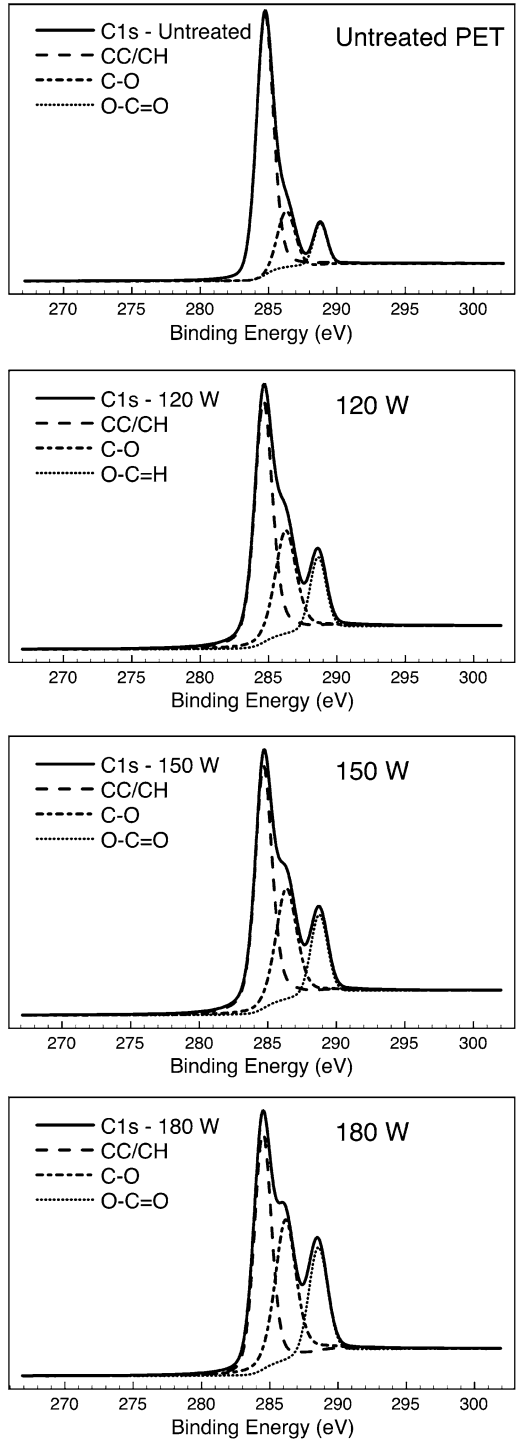
Table 5 Atomic % of species on PET surface before and after plasma treatment at various powers

Plasma treatment	Species (Atomic %)			WCA after 24 h
	CC/CH	C–O	O–C=O	
Untreated	68.8	18.6	12.6	93°
120 W	54.1	28.5	17.4	54°
150 W	51.3	29.7	19.0	52°
180 W	44.0	32.8	23.2	37°

contamination of hydrocarbons but this is inline with results reported previously [24]. The percentage of oxygen was seen to increase with an increase in power applied to the plasma as shown in Table 4. This increase in oxygen has the effect of reducing the relative % C in the samples.

Figure 12 shows the high-resolution C1s peaks of untreated PET and PET after plasma treatment at 120, 150 and 180 W respectively. The untreated PET sample's spectrum is deconvoluted into three components: a peak at 284.8 eV, representing C–C and C–H bonds (carbon atoms in a phenyl ring), a second peak representing C–O at 286.4 eV (methylene carbon atoms bonded to oxygen) and a third peak at 288.8 due to O–C=O bonds (ester carbon bonds) [24, 38]. In agreement to previous studies of PET processed at 27.12 MHz [25, 35], the C1s peak of the PET undergoes significant change after plasma treatment due to newly formed surface bonds. These spectra can also be deconvoluted into three sub-peaks at 284.8, 286.4 (120 and 150 W plasmas) 286.5 (180 W plasma) and 288.8 eV. The relative areas of these peaks are summarised in Table 4. The results indicate that a decrease of intensity occurs for C–C/C–H bonds (284.8 eV) post plasma treatment (the higher the plasma power the larger the decrease). C–O (286.4/5 eV) bonds increase in intensity after plasma activation with the sample processed at the highest plasma power experiencing the largest increase. The O–C=O bonds, at 288.8 eV, also undergo significant change in intensity after plasma processing with intensities nearly doubling for the 180 W sample. These observations can be explained by the fact that atmospheric plasmas mainly alter C–C and C–H bonds on the PET surface [38].

Surface activation is largely due to the incorporation of oxygen into the PET surface due to surface bond scission by the plasma forming C–O and O–C=O groups [24]. These newly formed polar groups lead to the increase in surface energy and reduction of WCA mentioned earlier and have previously been found on the surfaces of plasma treated PET. As the XPS analysis was conducted 24 h post activation it is interesting to compare the WCA of the polymers also measured at this point in time (Table 5). The WCA for the polymers was demonstrated to decrease with plasma power (and so with atomic oxygen surface composition).

Conclusion

This study investigates the performance of the SurFx source for the activation of PET using a He–O$_2$ plasma. The influence of processing parameters such as system input power, CNC speed and gap height, on the level of plasma surface activation, based on WCA measurements were investigated. Of these parameters system power was found to most influence WCA. The maximum reduction in WCA for PET was achieved using treatment powers of 180 W with a CNC speed of 30 mm s^{-1} and a 5 mm gap height, where WCA

was reduced from 93° to 34°. A relatively homogeneous reduction in WCA (34° to 47°) was demonstrated in this study after a single pass, under the 5 cm diameter jet source orifice.

Thermal image analysis and optical emission spectroscopy (OES) were obtained to determine the effect of both the heating and active species have on the polymer activation. Analysis of results obtained using these two techniques was compared at different system powers, locations along the plasma plume and at different times. The experiment has confirmed that OES can be used as an accurate diagnostics tool for determining plasma gas temperatures.

OES analysis demonstrated the increase in atomic species intensities with increased applied plasma power. The effect of this, according to XPS analysis of the PET samples, is an increase in oxygen content formed on the surfaces of plasma treated samples. This increase in oxygen results in lower WCAs for the PET. Normalised WCA measurements, along with the OH and H_α intensities obtained from optical emission spectroscopy, when plotted against power, show very similar trends indicating that H_α and OH may play a key role in the surface activation of polymers in helium discharges and have the potential to be used for real-time monitoring of WCA.

References

1. Deilmann M, Halfmann H, Steves S, Bibinov N, Awakowicz P (2009) Silicon oxide permeation barrier coating and plasma sterilization of PET bottles and foils. Plasma Process Polym 6(S1):S695–S699
2. Topala I, Dumitrascu N, Pohoata V (2008) Influence of plasma treatments on the hemocompatibility of PET and PET plus TiO(2) films. Plasma Chem Plasma Process 28(4):535–551
3. Fang Z, Qiu Y, Wang H (2004) Surface treatment of polyethylene terephthalate film using atmospheric pressure glow discharge in air. Plasma Sci Technol 6(6):2576–2580
4. Pu FR, Williams RL, Markkula TK, Hunt JA (2002) Expression of leukocyte-endothelial cell adhesion molecules on monocyte adhesion to human endothelial cells on plasma treated PET and PTFE in vitro. Biomaterials 23(24):4705–4718
5. Ademovic Z, Wei J, Winther-Jensen B, Hou X, Kingshott P (2005) Surface modification of PET films using pulsed AC plasma polymerisation aimed at preventing protein adsorption. Plasma Process Polym 2(1):53–63
6. Shenton MJ, Lovell-Hoare MC, Stevens GC (2001) Adhesion enhancement of polymer surfaces by atmospheric plasma treatment. J Phys D Appl Phys 34(18):2754–2760
7. Zanini S, Muller M, Riccardi C, Orlandi M (2007) Polyethylene glycol grafting on polypropylene membranes for anti-fouling properties. Plasma Chem Plasma Process 27(4):446–457
8. Bigan M, Bigot J, Mutel B, Coqueret X (2008) Grafting of copolymer styrene maleic anhydride on poly(ethylene terephthalate) film by chemical reaction and by plasma method: optimization of the grafting reaction using experimental design. Appl Surf Sci 254(8):2300–2308
9. Thyen R, Weber A, Klages CP (1997) Plasma-enhanced chemical-vapour-deposition of thin films by corona discharge at atmospheric pressure. Surf Coat Technol 97(1):426–434
10. Żenkiewicz M, Richert J, Rytlewski P, Moraczewski K (2009) Some effects of corona plasma treatment of polylactide/montmorillonite nanocomposite films. Plasma Process Polym 6(S1):S387–S391
11. Onsuratoom S, Rujiravanit R, Sreethawong T, Tokura S, Chavadej S (2010) Silver loading on DBD plasma-modified woven PET surface for antimicrobial property improvement. Plasma Chem Plasma Process 30(1):191–206
12. Borris J, Dohse A, Hinze A, Thomas M, Klages C-P, Möbius A, Elbick D, Weidlich E-R (2009) Improvement of the adhesion of a galvanic metallization of polymers by surface functionalization using dielectric barrier discharges at atmospheric pressure. Plasma Process Polym 6(S1):S258–S263

13. Dowling DP, O'Neill FT, Langlais SJ, Law VJ (2011) Influence of dc pulsed atmospheric pressure plasma jet processing conditions on polymer activation. Plasma Process Polym 8(8):718–727

14. Oteyaka MO, Chevallier P, Turgeon S, Robitaille L, Laroche G (2012) Low pressure radio frequency ammonia plasma surface modification on poly(ethylene terephthalate) films and fibers: effect of the polymer forming process. Plasma Chem Plasma Process 32(1):17–33

15. Orhan M, Kut D, Gunesoglu C (2012) Improving the antibacterial property of polyethylene terephthalate by cold plasma treatment. Plasma Chem Plasma Process 32(2):293–304

16. Yang S, Gupta MC (2004) Surface modification of polyethyleneterephthalate by an atmospheric-pressure plasma source. Surf Coat Technol 187(2):172–176

17. Dowling DP, Ramamoorthy A, Rahman M, Mooney DA, MacElroy JMD (2009) Influence of atmospheric plasma source and gas composition on the properties of deposited siloxane coatings. Plasma Process Polym 6(S1):S483–S489

18. Dowling DP, Twomey B, Byrne G, O'Neill L, O Hare L (2005) Deposition of functional coatings using an in-line atmospheric pressure plasma apparatus. In: Proceedings of the 48th annual conference—SVC, 2005. pp. 214–218

19. Lommatzsch U, Pasedag D, Baalmann A, Ellinghorst G, Wagner H-E (2007) Atmospheric pressure plasma jet treatment of polyethylene surfaces for adhesion improvement. Plasma Process Polym 4(S1):S1041–S1045

20. Arefi-Khonsari F, Tatoulian M, Bretagnol F, Bouloussa O, Rondelez F (2005) Processing of polymers by plasma technologies. Surf Coat Technol 200(1):14–20

21. Arefi-Khonsari F, Kurdi J, Tatoulian M, Amouroux J (2001) On plasma processing of polymers and the stability of the surface properties for enhanced adhesion to metals. Surf Coat Technol 142–444:437–448

22. Yang L, Chen J, Guo Y, Zhang Z (2009) Surface modification of a biomedical polyethylene terephthalate (PET) by air plasma. Appl Surf Sci 255(8):4446–4451

23. Nwankire C, Law V, Nindrayog A, Twomey B, Niemi K, Milosavljević V, Graham W, Dowling D (2010) Electrical, thermal and optical diagnostics of an atmospheric plasma jet system. Plasma Chem Plasma Process 30(5):537–552

24. Vesel A, Mozetic M, Zalar A (2007) XPS study of oxygen plasma activated PET. Vacuum 82(2):248–251

25. Vesel A (2011) Activation of polymer polyethylene terephthalate (PET) by exposure to Co2 and O2 plasma. Mater Technol 45(2):121–124

26. Junkar I, Vesel A, Cvelbar U, Mozetifç M, Strnad S (2009) Influence of oxygen and nitrogen plasma treatment on polyethylene terephthalate (PET) polymers. Vacuum 84(1):83–85

27. Carosio F, Alongi J, Frache A (2011) Influence of surface activation by plasma and nanoparticle adsorption on the morphology, thermal stability and combustion behavior of PET fabrics. Eur Polym J 47(5):893–902

28. Hocine D, Belkaid MS, Pasquinelli M, Escoubas L, Simon JJ, Rivière GA, Moussi A (2013) Improved efficiency of multicrystalline silicon solar cells by TiO2 antireflection coatings derived by APCVD process. Mater Sci Semicon Proc 16(1):113–117

29. Wang J, Chen JY, Yang P, Leng YX, Wan GJ, Sun H, Zhao AS, Huang N, Chu PK (2006) In vitro platelet adhesion and activation of polyethylene terephthalate modified by acetylene plasma immersion ion implantation and deposition. Nucl Instrum Meth B 242(1–2):12–14

30. Yang M-R, Chen K-S, Tsai J-C, Tseng C–C, Lin S-F (2002) The antibacterial activities of hydrophilic-modified nonwoven PET. Mater Sci Eng C 20(1–2):167–173

31. Vassallo E, Cremona A, Ghezzi F, Ricci D (2010) Characterization by optical emission spectroscopy of an oxygen plasma used for improving PET wettability. Vacuum 84(7):902–906

32. Kravets L, Dmitriev S, Gilman A, Drachev A, Dinescu G (2005) Water permeability of poly(ethylene terephthalate) track membranes modified by DC discharge plasma polymerization of dimethylaniline. J Membr Sci 263(1–2):127–136

33. Dowling DP, Tynan J, Ward P, Hynes AM, Cullen J, Byrne G (2012) Atmospheric pressure plasma treatment of amorphous polyethylene terephthalate for enhanced heatsealing properties. Int J Adhes Adhes 35:1–8

34. Lam YL, Kan CW, Yuen CW (2011) Effect of oxygen plasma pretreatment and titanium dioxide overlay on flame retardant finished cotton fabrics. BioResources 6(2):1454–1474

35. Gonzalez E 2nd, Barankin MD, Guschl PC, Hicks RF (2008) Remote atmospheric-pressure plasma activation of the surfaces of polyethylene terephthalate and polyethylene naphthalate. Langmuir 24(21):12636–12643

36. Li Y, Sun J, Yao L, Ji F, Peng S, Gao Z, Qiu Y (2012) Influence of moisture on effectiveness of plasma treatments of polymer surfaces. J Adhes Sci Technol 26(8–9):1123–1139

37. Homola T, Matousek J, Hergelova B, Kormunda M, Wu LYL, Cernak M (2012) Activation of poly(ethylene terephthalate) surfaces by atmospheric pressure plasma. Polym Degrad Stab 97(11):2249–2254
38. Kostov KG, dos Santos ALR, Honda RY, Nascente PAP, Kayama ME, Algatti MA, Mota RP (2010) Treatment of PET and PU polymers by atmospheric pressure plasma generated in dielectric barrier discharge in air. Surf Coat Technol 204(18–19):3064–3068
39. Pellerin S, Cormier JM, Richard F, Musiol K, Chapelle J (1996) A spectroscopic diagnostic method using UV OH band spectrum. J Phys D Appl Phys 29(3):726–739
40. Mortazavi M, Nosonovsky M (2012) A model for diffusion-driven hydrophobic recovery in plasma treated polymers. Appl Surf Sci 258(18):6876–6883
41. Strom G, Fredriksson M, Stenius P (1987) Contact angles, work of adhesion, and interfacial tensions at a dissolving Hydrocarbon surface. J Colloid Interf Sci 119(2):352–361
42. Owens DK, Wendt RC (1969) Estimation of the surface free energy of polymers. J Appl Polym Sci 13(8):1741–1747
43. Milosavljevic V, Ellingboe AR, Daniels S (2011) Influence of plasma chemistry on oxygen triplets. Eur Phys J D 64(2–3):437–445
44. Stallard C, McDonnell K, Onayemi O, O'Gara J, Dowling D (2012) Evaluation of protein adsorption on atmospheric plasma deposited coatings exhibiting superhydrophilic to superhydrophobic properties. Biointerphases 7(1–4):1–12